Diffractive and Jet Physics with a Forward PLUG Calorimeter at ZEUS

A. Bamberger[a], S. Eisenhardt[a], H. Heßling[b], H. Raach[a], S. Wölfle[a]

[a] Universität Freiburg, Fakultät für Physik, D-79104 Freiburg, FRG
[b] Deutsches Elektronen-Synchrotron DESY, D-22603 Hamburg, FRG

Abstract: It is suggested to upgrade the forward ZEUS calorimeter in the current beam hole by a FPLUG calorimeter. The foreseen layout of the FPLUG would increase the acceptance of the ZEUS detector in the forward direction by 1.6 units in pseudorapidity. The calorimetric properties of the FPLUG are studied and its potential for diffractive physics and jet physics is analyzed.

1 Introduction

The complete coverage of phase space in the physics of lepton-proton scattering at HERA is one of the objectives of a multipurpose detector such as ZEUS or H1.
Since the observation of diffractive processes in deep inelastic scattering events with rapidity gaps have been interesting in various ways. An increase in acceptance is advantageous for the study of these processes. The very forward detection by the forward neutron spectroscopy (e.g. FNC at ZEUS) and the leading proton spectrometers (e.g. LPS at ZEUS) is successfully implemented. Their acceptance covers typically small momentum transfers, since they are integrated into the beam guiding systems. However, the transition region of forward calorimetry and the beam guiding systems is more difficult to equip with detectors because a number of boundary conditions have to be met. One option is the implementation of detectors wherever the beam elements allow to do so. This has been pursued by H1 and realised as a cascaded version of calorimetry. The other option is the implementation of the forward detection by "smooth" continuation of the calorimetry near the beam modifying the beam pipe and some of the vital elements as collimators and pumps.
Here we present a part of the results of this activity. The possible realisation (section 2) and the improvement for the detection of scattering processes are discussed. Among a variety of possible fields of interest we concentrate on the detection of diffractive DIS via the calorimetric measurement of diffractively produced masses (section 3) and the jet detection in the forward direction (section 4).

2 The FPLUG Calorimeter

2.1 Physics Requirements and Layout of the FPLUG Calorimeter

The requirements for a FPLUG calorimeter are:

- angular acceptance as close as possible at the proton beam,
- energy resolution similar to the energy resolution of the main calorimeters,
- small distortion of the response at the boundary of the calorimeters,
- small amount of dead material in front of the FPLUG.

The most efficient way to realise this is a FPLUG calorimeter integrated into the existing calorimeter. Transition effects at the boundary between the calorimeters are minimized this way. Shadowing effects as would be the case in a cascaded version are avoided. The cross talk due to leakage, especially for the hadronic cascade, is intrinsically present. The closest approach to the proton and electron beam is limited by its sizes, the various injection conditions and synchrotron radiation fan accompanying the electron beam, in our case typically 2 cm.
The requirements for the angular resolution are moderate, since the invariant mass resolution of M_X is mainly determined by the energy resolution. However, the angular resolution and granularity is of importance for the separation of diffractively excited proton system.

2.2 General Layout

The FPLUG calorimeter would be positioned inside the current beam hole of the ZEUS forward calorimeter (FCAL) with a dimension of 20×20 cm^2. Leaving a hole for the beam pipe of 4×4 cm^2 the acceptance in pseudorapidity η could be increased from 3.8 to 5.4 at the front face of the calorimeter.

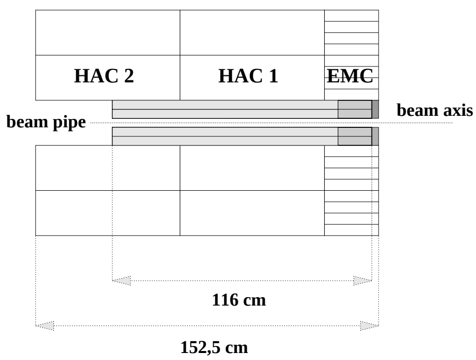

Figure 1: *Layout of the FPLUG inside FCAL (DU–version).*

The general layout of the FPLUG calorimeter inside the ZEUS FCAL is given in Fig. 1. A possible realization of the FPLUG calorimeter could be a spaghetti type calorimeter with tungsten as absorber medium. Tungsten has a very short nuclear interaction length λ of 10.3 cm which would allow for a rather compact hadron calorimeter. Space considerations would limit the amount of fibres to 10%.
The scintillating fibres would run along the beam axis and could be read out both from the direction of the interaction point and from the back, thus defining the electromagnetic and

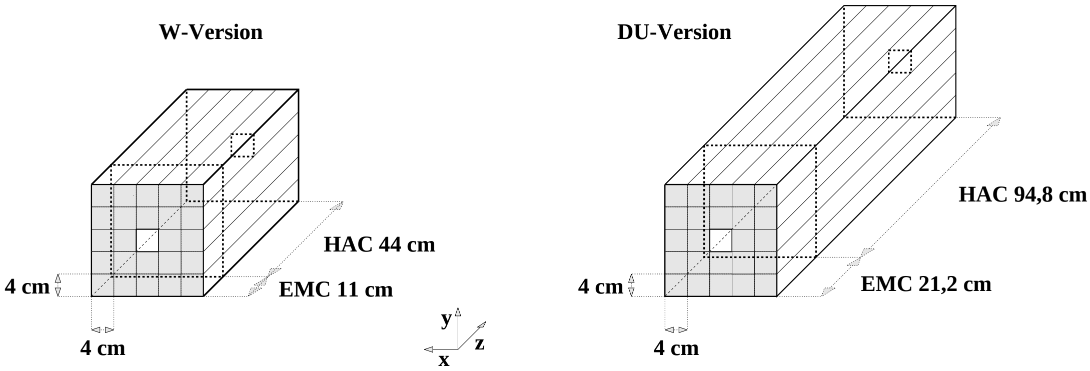

Figure 2: *Readout granularity of the FPLUG.*
Only the lognitudinal layout differs between W and DU–version.

hadronic sections of the calorimeter. The electromagnetic part would have the length of 1 λ, the hadronic part of 4 λ, giving a total length of 55 cm. This is two interaction lengths shorter than the FCAL, but sufficient as will be shown in Fig. 5
The usage of scintillating fibres would allow a flexible readout granularities. Our studies were employing a cell structure of 5×5 with a square cross section of each cell of 4×4 cm^2 and the center cell replaced by the beam pipe, cf. Fig. 2.

2.3 Monte Carlo Studies of the Calorimetric Properties

General features of a W–scintillating fibres calorimeter such as sampling fraction, energy resolution and leakage were studied by a "stand alone" simulation. In order to save computing time the fibre geometry was replaced by a sandwich structure of alternating layers of 9 mm W and 1 mm polystyrene as scintillator material preserving the 10% of active volume foreseen.
The simulation of the electromagnetic showers was performed with the GEANT 3.21 package [1]. For a detailed simulation of hadronic showers we used the GEANT–GCALOR interface [2]. The CALOR89 program package simulates hadronic interactions down to 1 MeV for nucleons and charged pions and into thermal regions for neutrons, for higher energies the FLUKA model [3] is employed.
The transport of neutrons down to thermal energies and the use of cross section tables for the various elements is expected to make the simulation of the response of hadronic calorimeters (which is especially sensitive to neutrons) rather reliable, cf. Ref. [4].
The response of the calorimeter was determined by hitting a very large calorimeter with monoenergetic particles (electrons or positive pions), incident at the center, perpendicular to the layer orientation. Sampling fractions are energy dependent and lie in the range of 0.7%, cf. Fig. 3a, the calorimeter is slightly overcompensating.
The electromagnetic energy resolution could be parametrized in the following form

$$\frac{\sigma_E}{E} = \frac{(31.1 \pm 1.2)\,\%}{\sqrt{E[\mathrm{GeV}]}} \ .$$

A detailed study that took into account the precise fibre geometry (1 mm diameter, 3.2 mm spacing) showed a more complicated behaviour due to the small number of fibres participating in an electromagnetic shower. This was confirmed by test beam measurements [5].

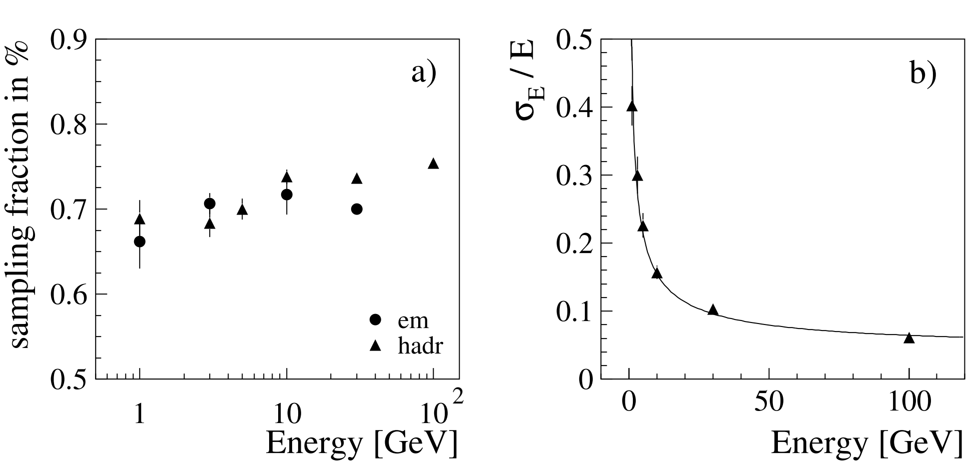

Figure 3: *a) Electromagnetic and hadronic sampling fractions,*
b) Hadronic energy resolution.

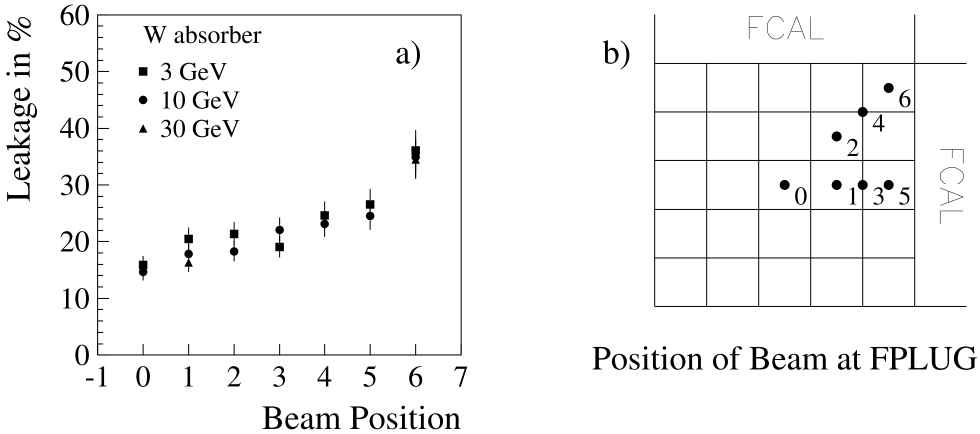

Figure 4: *a) Energy dependent leakage of W–FPLUG into FCAL.*
b) Incident points for leakage study on W and DU–FPLUG.

The energy resolution for hadronic showers was found to be

$$\frac{\sigma_E}{E} = \frac{(45.2 \pm 1.7)\,\%}{\sqrt{E[\mathrm{GeV}]}} \oplus (4.6 \pm 0.6)\,\% \ ,$$

with the two contributions added in quadrature.
As the foreseen dimensions of the FPLUG are rather small for a hadronic calorimeter, especially in lateral direction, leakage into the FCAL cannot be neglected. Fig. 4a gives the leakage[1] for various energies from the FPLUG into the FCAL. The different entrance positions of the beam are indicated in Fig. 4b.
The energy resolution as a function of the calorimeter length was also extracted from the simulations. For this, no hole for the beam pipe was modelled, the particles were hitting the FPLUG at the center (point 0 in Fig. 4b). The results for 10, 30 and 100 GeV are shown in Fig. 5. One can see that there is no significant gain in the energy resolution for $\lambda > 5$.

[1]Leakage always denotes the fraction of energy deposited in the FCAL divided by the total energy deposition both in FPLUG and FCAL.

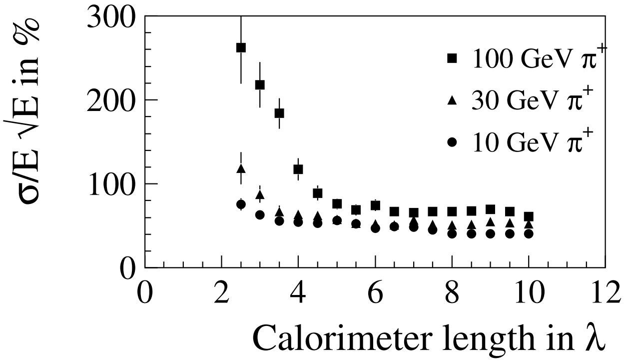

Figure 5: *Dependence of energy resolution on calorimeter length.*

2.4 Simulation of the FPLUG within the ZEUS Detector

The physics results presented in the next sections were gained with a simulation routine where the FPLUG calorimeter was implemented in the general ZEUS Monte Carlo routine MOZART. As a detailed simulation of hadronic showers in tungsten within the MOZART environment would be too time consuming and not reliable[2] we chose the same DU–scintillator "porridge" which is used as tracking material for the FCAL. The length of the FPLUG was adapted to the larger interaction length of 23.3 cm by increasing it to 116 cm as displayed in Fig. 1, again corresponding to 5 λ.
To take into account dead material (pump and flanges), a layer of 3 cm iron was situated just in front of the FPLUG.

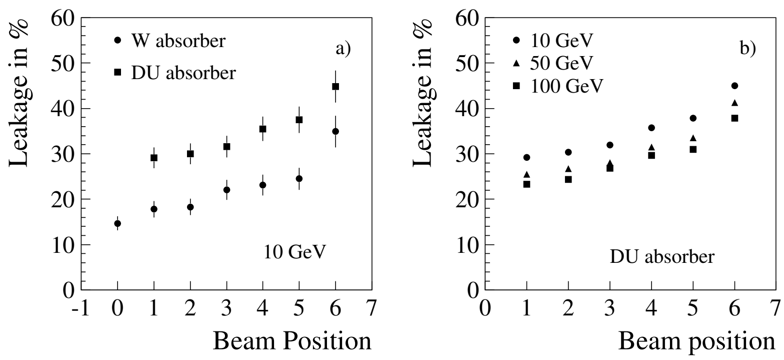

Figure 6: *a) Leakage from the FPLUG into FCAL for W and DU–absorber.*
b) Leakage from a DU–FPLUG into FCAL for different energies.
For the beam positions cf. Fig. 4b.

An idea of the different behaviour of tungsten and uranium as absorber can be obtained by looking at figure Fig. 6a where the larger leakage of DU with respect to W for 10 GeV pions is displayed. The lower leakage of the W configuration is caused by the smaller shower spread due to the higher density. The energy dependence of the leakage for DU is plotted in Fig. 6b.

2.5 Monte Carlo Programs

The relevant event generators are DJANGO6 and POMPYT2.2 [6] for the non-diffractive and diffractive events, respectively. DJANGO6 2.1 (2.2) [7] is an interface between LEPTO 6.1

[2] The GEANT version in MOZART is too old to be used with the GCALOR interface.

(6.3) [8] and HERACLES 4.4 (4.5) [9]. In this section the non-diffractive process $ep \to eX$ is simulated with LEPTO6.1. The following parameters for POMPYT were taken: slope of the pomeron exchange to be 8 GeV^{-2}, no excitation of the diffractive scattered proton system, flat pomeron structure function $F_2^{I\!P}(\beta, Q^2) = 1$. Note, that for this investigation the proton dissociation option within POMPYT was switched OFF. The version used for MOZART was NUM12.3, which does include the C4 collimator for realistic comparison.

3 Diffractive Physics

Diffractive physics in deep inelastic electron–proton scattering has become popular since rapidity gap events have been identified at HERA in 1993 [10].
The discrimination of diffractive events from normal DIS can be achieved in different ways, for example by rapidity gaps or by the invariant mass accepted by the detector being small as compared with "normal" deep inelastic events. In the following we assume the latter definition. The topology of diffractively produced events is of major interest because the exchange of a pomeron at the proton vertex reveals QCD properties of the exchanged object.
The interest in the extention of the acceptance of the calorimetric detector has many reasons, of which in this section mainly the diffractive physics is discussed. Aspects of non-diffractive physics are insofar relevant as they represent the major part of the cross section and cover in certain kinematical ranges the diffractive events as background.

3.1 Outline of Physics Processes

3.1.1 Definition of the Variables used

The diagrams of the physics processes and some kinematic variables are indicated in Fig. 7. The mass of the hadronic final state, W, can be expressed in terms of Q^2 and Bjorken–x:

$$W^2 = Q^2(1/x - 1) + m_p^2 \approx Q^2/x \quad \text{for} \quad x \ll 1. \tag{1}$$

The following argument uses the rapidity variable y approximated by the pseudorapidity η:

$$y = \frac{1}{2} \ln \frac{E + p_{||}}{E - p_{||}} \qquad \text{and} \qquad \eta = -\ln \tan \frac{\theta}{2},$$

where $\tan\theta = p_t/p_z$ and $\theta, E, p_{||}$ and p_t are the angle with respect to the proton beam, the particle energy, the longitudinal and transversal momentum.

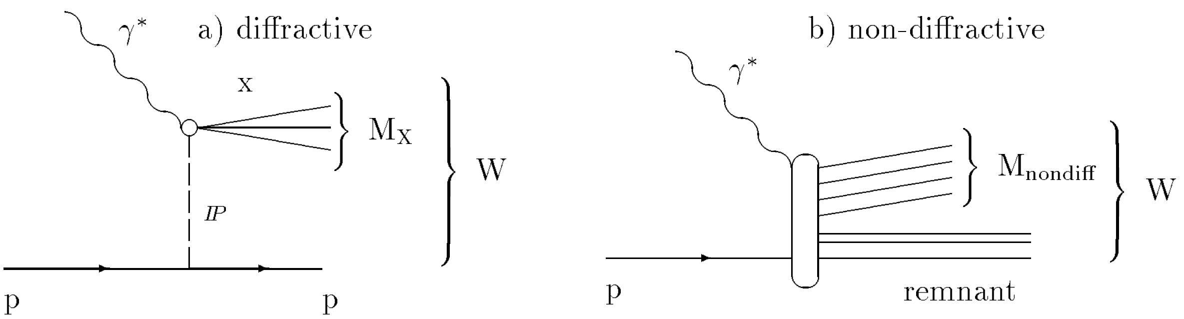

Figure 7: *Diagrams for the subprocess of diffractive scattering (a) and non-diffractive scattering (b). The M_X and $M_{nondiff}$ are the invariant masses accepted by the detector for the respective process.*

3.1.2 Deep Inelastic scattering in the Longitudinal Phase Space Model

Non-diffractive final state may be described as a uniformly distributed particle density in rapidity, $dn/dy = const$, except near the kinematical limits y_{min} and y_{max}. In the central range y may be approximated with η, which is actually the measured variable.
The total hadronic mass W, as given in Eq. 1, can also be expressed in this description as $W^2 = c \cdot \exp(y_{max} - y_{min})$, with c being a constant.
If the calorimetric detector provides good hermeticity in the backward direction but has an acceptance limit in forward direction at $y_{CAL} \approx 3.8 < y_{max}$ the observed invariant mass is $M^2_{nondiff} = c \cdot \exp(y_{CAL} - y_{min})$, where CAL denotes the total calorimetric detector. So the observed mass is smaller than W by the amount lost within the forward beam pipe, corresponding to the factor $\exp[(y_{max} - y_{CAL})/2]$, cf. Fig. 8 (non-diffractive case).

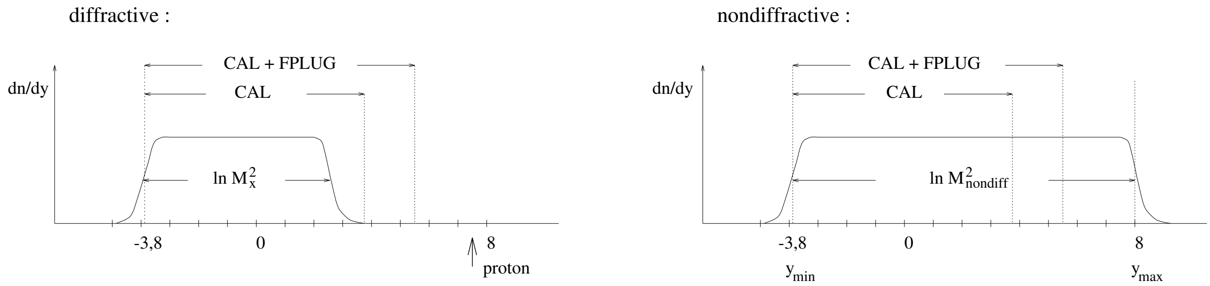

Figure 8: *Sketch of the distributions in rapidity for diffractive (left) and non-diffractive DIS (right) for the detector configurations with/without FPLUG calorimeter.*

If the acceptance in the forward direction is improved by the insertion of a FPLUG by ≈ 1.5 units in rapidity the observed non-diffractive mass distribution is shifted by the amount of

$$\Delta \ln M^2_{nondiff} = y_{CAL+FPLUG} - y_{CAL} = 1.5, \tag{2}$$

where $y_{CAL+FPLUG}$ means the maximum accepted rapidity of the combined system CAL and FPLUG. In other terms $M^{CAL+FPLUG}_{nondiff}/M^{CAL}_{nondiff} = 2.12$. This way the invariant mass spectrum of non-diffractive events is shifted. As will be shown below, the diffractive events having a rapidity gap between the particles of the diffractively produced system and the scattered proton system will not be affected by the increase of the acceptance [11], resulting in a considerably better separation of these two processes.

3.1.3 Deep Inelastic Diffractive Scattering

Diffractive inelastic scattering is described by the subprocess $\gamma^* p \rightarrow Xp$. The relevant variables are Q^2, x and M_X. The events are characterised by the exchange of a colorless object between the system X and the proton. Its signature is a large rapidity gap between the hadrons of X and the proton which is scattered with small momentum transfer, see Fig. 7a.
The rapidity gap is the essential feature of the diffractive scattering process, see Ref. [12]. Due to the rapidity gap the M_X is virtually independent of the acceptance of the calorimeter in the forward direction y_{CAL} or $y_{CAL+FPLUG}$, see Fig. 8 (diffractive case). In contrast to the Eq. 2 one expects $M_X^{CAL+FPLUG}/M_X^{CAL} \approx 1$. Therefore the separation between diffractive and non-diffractive processes is the better the closer the acceptance of the detector approaches the proton system.
Due to fluctuations, rapidity gap events do occur also in non-diffractive events, but they are, with increasing rapidity gap, exponentially suppressed. The signature of diffractive events is

that they are not suppressed with increasing rapidity gap. This results in a plateau-like behaviour of the M_X-distribution in terms of $\ln M_X^2$ for low values of M_X for diffractive events [13]. The plateau is followed, for higher masses M_X, by a peak which is due to non-diffractive DIS. In the overlap region the non-diffractive DIS may be described as an exponential fall off with decreasing M_X.

3.1.4 Energy Dependence of Diffractive DIS

The differential cross section of diffractive events, extracted by subtraction of the exponential fall off the non-diffractive DIS events, shows an almost linear rise with W. The W dependence can be formulated in terms of Regge exchange

$$\frac{d\sigma_{\gamma^* p \to XN}(M_X, W, Q^2)}{dM_X} \propto (W^2)^{(2\alpha_{I\!P}-2)},$$

where $\alpha_{I\!P}$ is the t-averaged pomeron trajectory. Experimentally it is found that $\alpha_{I\!P} = 1.23 \pm 0.02(stat.) \pm 0.04(syst.)$ [11], which is substantially larger than expected from soft hadron-hadron scattering.
In view of various models describing the energy dependence, see for instance Ref. [14], it is of great importance to increase the mass range of M_X to higher accessible values, in order to explore whether there is a transition from hard to soft exchange as M_X increases.

3.1.5 Jet Structure of Diffractive DIS

The structure of the system X produced by the process

$$\gamma^* I\!P \to X$$

might be used to distinguish between different reaction mechanisms.
For instance in the aligned jet model [12], as well as in the LO process of POMPYT [6], a two-jet final state is expected. On the other hand a hard gluon emission will result in a final state of three partons. A clear distinction of a three–jet final state from a two–jet final state can be achieved only if the mass of the diffractive system M_X is sufficiently large.

3.2 Diffractive and Non-diffractive Event Simulation

As shown above in Sec. 3.1.3 the separation of the diffractive from non-diffractive events can be accomplished by the size of the invariant mass accepted by the detector. The peak position of the non-diffractive invariant mass spectrum depends crucially on the upper bound of the η-acceptance. The applied cuts follow the evaluation of the ZEUS data from reference [11]. Especially the noise cut-off results in a correction of the detected mass. In the following a correction factor of $1/0.68$ was applied to the mass scale M_X. The improvement of separation due to the insertion of the FPLUG can be seen in Fig. 9. The vertical line indicates M_X, where the signal to background ratio is near one. The improvement due to the insertion of the FPLUG is a factor of two. This way, masses of 22 GeV for $W = 150$ GeV and 36 GeV for $W = 245$ GeV are accessible. It should be mentioned that in this plot the events at $W \neq 150$ GeV are rescaled in M_X with the relation $M_X/W = const.$
In order to demonstrate that these high masses are efficiently accepted for diffractive DIS by the improved detector the maximum η of the most forward going hadron at the hadron level is

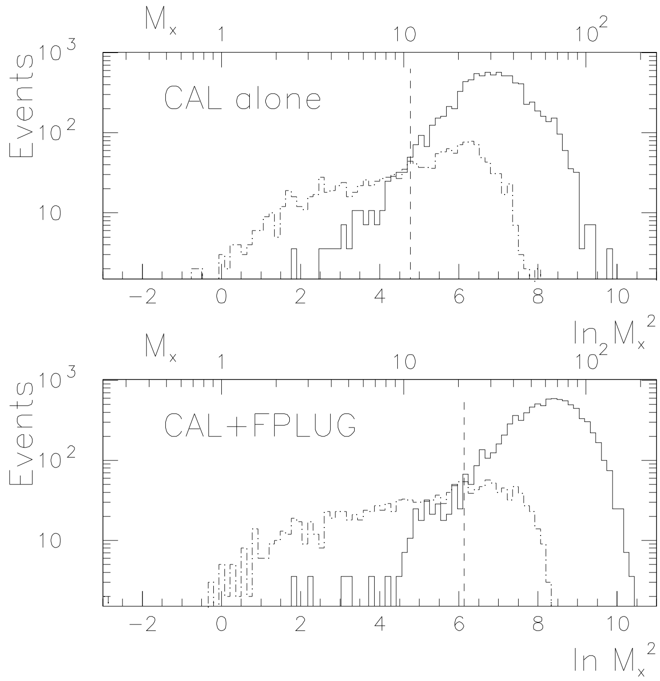

Figure 9: *The distribution of* $\ln(M_X^2)$ *for diffractive (dashed) and non-diffractive events (solid line) for an average* $\bar{W} = 150$ GeV. M_X *is corrected to the hadron level. Top: for the ZEUS detector with full calorimetry. Bottom: for the ZEUS detector with the addition of the FPLUG calorimeter. The gain for detection of diffractive events is a factor 2.0 in* M_X.

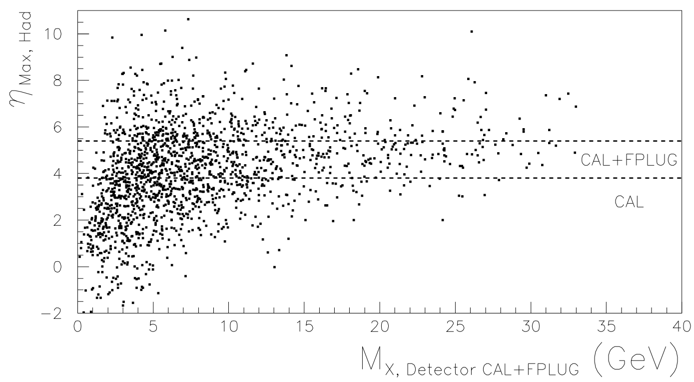

Figure 10: *The distribution of pseudorapidity* η_{max} *of the most forward going particle produced at hadron level versus reconstructed* M_X *on detector level (CAL+FPLUG) in diffractive DIS. See Sec. 2.5 for details on the event generation.*

plotted as a function of the reconstructed M_X at the detector level, see Fig. 10. The distribution shows that the most forward going hadron of a diffractive DIS event is accepted by the CAL alone in 42% of the calculated events, but it is accepted in 75% of the calculated events if the FPLUG is added and the acceptance limit is raised to $\eta = 5.4$.

It should be noted that the use of the FPLUG as an anticounter, establishing a rapidity gap between $\eta = 3.8$ and $\eta = 5.4$, accepts only $M_X < 18$ GeV for $W = 150$ GeV. The cut used for vetoing minimum ionizing particles is 400 MeV. This is an important fact showing that different selection criteria for diffractive events accept different topology.

Concerning the simulation of a "cascaded" version of the plug calorimeter, which also has been performed, the following facts have been observed. Dead material as being present with the collimator in front change also the vetoing efficiency. This in turn means a high sensitivity to the detailed description of the dead material in the simulation.

3.3 Conclusion

There are a number of reasons to have an extended acceptance of the calorimetric measurement of the final state for diffractive events. A FPLUG calorimeter inserted into the existing forward calorimeter of ZEUS increases the separation of diffractive from non-diffractive events dramatically. It therefore would allow for the exploration of the W dependence and its interpretation in terms of pomeron exchange within the frame of Regge model and it would allow for the investigation of the final states of the system X through jet analysis.
The geometrical increase of the acceptance is 1.6 units in η for this simulation. The effective increase in $\ln M_x^2$ amounts to 1.35 units, somewhat smaller than expected from the geometrical acceptance. Remember that the situation "without a plug" has an inert collimator in place of the plug. The effects are absorption and rescattering changing the energy flow in this rapidity intervall by as much as a factor 2. The main result is that masses M_X up to 36 GeV are obtainable in diffractively produced events with the capability of the investigation of their topology. It should be mentioned that the investigation of excitation of the diffractively scattered proton is an additional subject of interest.

4 Jets in Deep Inelastic Scattering

In this section the influence of a FPLUG Calorimeter on forward jet physics in deep inelastic scattering is investigated using the *JADE algorithm* [15] and the *extended JADE algorithm* [16]. In the following the JADE algorithm is applied in the reference frame of the ZEUS detector. The extended JADE algorithm is Lorentz invariant, contrary to the JADE algorithm which is applied in the reference frame of the ZEUS detector. The jet resolution parameter is set to $y_{\mathrm{cut}} = 0.02$.
The jets of an event are ordered with respect to their distance $d_{i,\mathrm{prot}}$ to the momentum of the proton beam. The jet with the smallest distance $d_{i,\mathrm{prot}}$ is called *remnant jet*. The *forward jet* is defined to be the non–remnant jet with the smallest distance to the proton beam. The forward jet is also called *first current jet*.
At the hadron level the JADE algorithm and the extended JADE algorithm are applied to the momenta of the particles of the hadronic final state (apart from the scattered lepton). At the detector level they are applied to the momenta of the calorimeter cells not assigned to the scattered lepton and to the momentum of the pseudoparticle which is given by the momentum of the hadronic activity lost in the beam pipes.
Forward jets are expected to be of importance, to find signatures of the BFKL evolution [17] and "Hot Spots" [18].
The FPLUG improves the acceptance of the ZEUS detector with respect to the forward jet of (2+1) jets. To show this, we study at the detector level the extension of the forward jet with respect to the pseudorapidity η using the JADE algorithm. In Fig. 11 a Monte Carlo scatter plot of the pseudorapidity η_{jet} of the forward jet versus $\Delta\eta = \eta_{\mathrm{cell}} - \eta_{\mathrm{jet}}$ is shown, where η_{cell} are the pseudorapidities of the detector cells which are recombined to the forward jet. As can be seen, the forward jets are reconstructed in the forward direction around $\eta_{\mathrm{jet}} = 4$ and a considerable part of cells of the forward jets belong to the FPLUG.
However, the improvement of the FPLUG on forward jet physics may be quite small. Consider the transverse momentum of the forward jet determined by the JADE algorithm. In Fig. 12 a

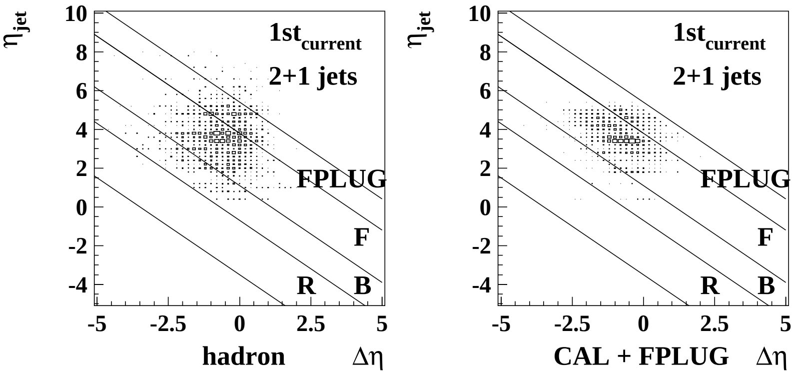

Figure 11: *Scatter plot of the pseudorapidity* $\eta_{\rm jet}$ *of the forward jet versus* $\Delta\eta = \eta_{\rm cell} - \eta_{\rm jet}$ *where* $\eta_{\rm cell}$ *are the pseudorapidities of the detector cells which are recombined to the forward jet. On the left hand side the hadron level is shown, on right hand side the detector level, using the Monte Carlo program DJANGO6 (version 2.1). Also indicated are the acceptance limits of the Rear Calorimeter (R), the Barrel Calorimeter (B), the Forward Calorimeter (F) and the FPLUG Calorimeter (FPLUG). The kinematic range is restricted to* $Q^2 > 7$ GeV^2.

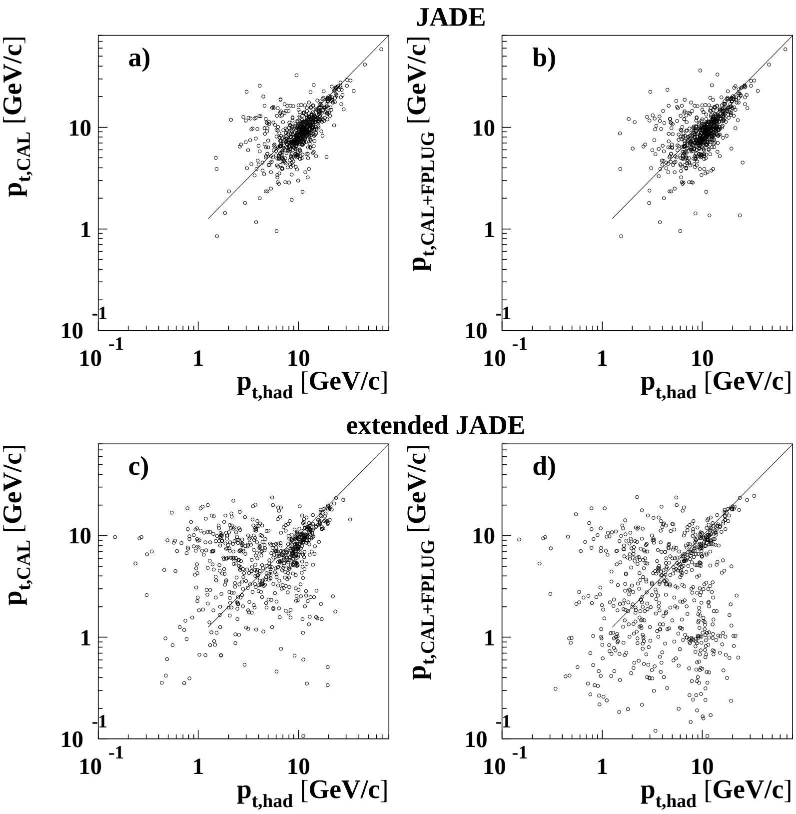

Figure 12: *Scatter plot of the transverse momentum of the forward jet: detector level versus hadron level without (a, c) and with (b, d) a FPLUG, using the Monte Carlo program DJANGO6 (version 2.2). For the scatter plots on the top the JADE algorithm is used, on the bottom the extended JADE algorithm. The kinematic range is restricted to* $Q^2 > 100$ GeV^2.

Monte Carlo scatter plot of the detector level versus the hadron level is shown without (a) and with (b) the FPLUG. By comparing Fig. 12a with Fig. 12b it can be seen that the transverse momentum is only very weakly influenced by the FPLUG.

An influence of the FPLUG on the transverse momentum of the forward jet is clearly observable, if the JADE algorithm is replaced by the extended JADE algorithm. Fig. 12c shows the Monte Carlo scatter plot (detector level versus hadron level) of the transverse momentum of the forward jet. A correlation is visible, but there are also many off–diagonal events in the left upper part around $p_{t,had} = 1$ GeV and $p_{t,CAL} = 10$ GeV. They originate in events which are identified as (2+1) jets at the hadron level but as (1+1) jets at the detector level. The forward jet of a (2+1) jet is mainly propagating into the forward direction, and it may happen that most of its energy is lost in the beampipe. In this case the energy depositions in the inner FCAL cells are too small to be identified as a jet and are recombined with the calorimeter cells in the central part of the detector to the current jet. This causes a jump in the transverse momentum of the forward jet between the hadron level and the detector level. Note that the transverse momentum of the current jet of a (1+1) jet is balanced by the transverse momentum of the scattered lepton and thus is of the order of Q.
The purity of the scatter plot of the transverse momentum of the forward jet is improved by a FPLUG calorimeter: Fig. 12d shows that the density of the off–diagonal events in the left upper part is reduced compared to Fig. 12c. On the other hand, an increase of off–diagonal events in the right lower part is observed stemming from events which are generated as (1+1) jets but reconstructed as (2+1) jets. Contrary to the off–diagonal events in the left upper part, the off–diagonal events in the right lower part can be removed by a cut on the transverse momentum.
The JADE algorithm seems to have a tendency to recombine a lot of the forward directed hadronic activity into the remnant jet. If the extended JADE algorithm is used, the forward activity is more likely resolved as a current jet.
In summary, an FPLUG Calorimeter improves forward jet physics, if the jets are determined with a jet algorithm which is sufficiently sensitive to the hadronic activity in the forward direction.

5 Summary

The investigation of improvement for physics detection by a FPLUG at the ZEUS detector yields:

- The accepted invariant masses of the diffractively produced system increases by a factor 2.0. This way masses as high as 36 GeV become accessible for the investigation of event topology in terms of jet analysis.

- Improved reconstruction of jets in the forward region using the JADE and the extended JADE algorithm. The sensitivity of hadronic activity in the η-range between 3.8 and 5.4 seems to be larger for the extended JADE algorithm. In this region additional hadronic activity by BFKL-processes and Hot Spots are expected.

There are a number of interesting topics not explicitly covered here, of which we mention: forward energy flow, double diffaction, multiple scattering in hard photo production, accepting events in hard photo production with larger rapidity gap than without FPLUG and separation of remnant jets from current jets.
In conclusion, the FPLUG will be very fruitfull for the understanding of various aspects of forward physics.

Acknowledgement

We thank the organizers of the workshop "Future at HERA" and the convenors of the working groups "Diffractive Hard Scattering" and "Jets and High E_T Phenomena" for their strong support.

References

[1] R. Brun and F. Carminati, *GEANT Detector Description and Simulation Tool*, CERN Program Library Long Writeup W5013 (1994).

[2] C. Zeitnitz and T.A. Gabriel, *The GEANT–CALOR Interface User's Guide*, 1994, unpublished.

[3] A. Fasso et al., *FLUKA 92*, Proceedings of the Workshop on Simulating Accelerator Radiation Experiments, Santa Fe (1993).

[4] C. Zeitnitz and T.A. Gabriel, *The GEANT–CALOR interface and benchmark calculations of ZEUS test calorimeters*, NIM **A349** (1994) 106.

[5] A. Bamberger et al., ZEUS Note in preparation (1996).

[6] POMPYT 1.0: P. Bruni and G. Ingelman, Proc. Europhysics Conf. on HEP, Marseilles 1993, 595.

[7] K. Charchuła, G.A. Schuler and H. Spiesberger, *DJANGO6*, version 1.1, Comp. Phys. Commun. **81** (1994) 381.

[8] G. Ingelman, *LEPTO*, version 6.1, in: Proceedings '*Physics at HERA*', vol. 3, W. Buchmüller, G. Ingelman (eds.), DESY Hamburg 1992.

[9] H. Spiesberger, *HERACLES*, version 4.4, unpublished program manual (1993); version 4.0 as described in A. Kwiatkowski, H.–J. Möhring and H. Spiesberger, Comp. Phys. Commun. **69** (1992) 155.

[10] ZEUS Collaboration, M. Derrick et al., Phys. Lett. **B315** (1993) 481;
ZEUS Collaboration, M. Derrick et al., Phys. Lett. **B338** (1994) 483;
H1 Collaboration, T. Ahmed et al., Nucl. Phys. **B429** (1994) 477.

[11] ZEUS Collaboration, M. Derrick et al., Z. Phys. **C70** (1996) 391.

[12] J.D. Bjorken, 1971 Int. Symp. Electron and Photon Interactions at High Energies, Cornell, 1971.

[13] ZEUS Collaboration, M. Derrick et al., Z. Phys. **C68** (1995) 569.

[14] J. Bartels, H. Lotter, M. Wüsthoff, DESY 96-026;
S.J. Brodsky et al., Phys. Rev. **D50** (1994) 3134.

[15] G. Kramer, DESY 82–029 (1982), published in Proc. of the 13th Spring Symp. on High Energy Physics, Bad Schwandau/GDR (1982);
JADE Collab., W. Bartel et al., Phys. Lett. **B119** (1982) 239;
JADE Collab., W. Bartel et al., Z. Phys. **C33** (1986) 22;
JADE Collab., S. Bethke et al., Phys. Lett. **B213** (1988) 235.

[16] H. Heßling, preprint DESY 95–069 (1995).

[17] L.N. Lipatov, Sov. J. Nucl. Phys. **23** (1976) 338;
E.A. Kuraev, L.N. Lipatov, V.S. Fadin, Sov. Phys. JETP **45** (1977) 199;
Y.Y. Balitskii, L.N. Lipatov, Sov. J. Nucl. Phys. **28** (1978) 822.

[18] A.H. Mueller and H. Navelet, Nucl. Phys. **B282** (1987) 727;
A.H. Mueller, Nucl. Phys. B (Proc. Suppl.) **18C** (1991) 125.